

---

# Variationally Inferred Sampling Through a Refined Bound for Probabilistic Programs

---

Víctor Gallego

Institute of Mathematical Sciences (ICMAT-CSIC),  
SAMSI (Duke University)

David Ríos Insua

## Abstract

A framework to boost efficiency of Bayesian inference in probabilistic programs is introduced by embedding a sampler inside a variational posterior approximation, which we call the refined variational approximation. Its strength lies both in ease of implementation and in automatically tuning the sampler parameters to speed up mixing time. Several strategies to approximate the *evidence lower bound* (ELBO) computation are introduced, including a rewriting of the ELBO objective. A specialization towards state-space models is proposed. Experimental evidence of its efficient performance is shown by solving an influence diagram in a high-dimensional space using a conditional variational autoencoder (cVAE) as a deep Bayes classifier; an unconditional VAE on density estimation tasks; and state-space models for time-series data.

## 1 Introduction

Probabilistic programming offers powerful tools for Bayesian modelling, a framework for describing prior knowledge and reasoning about uncertainty. A probabilistic programming language (PPL) can be viewed as a programming language extended with random sampling and Bayesian conditioning capabilities, complemented with an inference engine that produces answers to inference, prediction and decision making queries. Some examples are WinBUGS [1], Stan [2], or the recent Edward [3] and Pyro [4]. The machine learning and artificial intelligence communities are pervaded by models that can be expressed naturally through a PPL.

Variational autoencoders (VAE) [5] or hidden Markov models (HMM) [6] are two relevant examples.

If we consider a probabilistic program to define a distribution  $p(x, z)$ , where  $x$  are observations and  $z$  denote both latent variables and parameters, then we are interested in asking queries involving the posterior  $p(z|x)$ . This distribution is typically intractable but, conveniently, PPLs provide inference engines to approximate this distribution using Monte Carlo methods (e.g. particle Markov Chain Monte Carlo (MCMC) [7] or Hamiltonian Monte Carlo (HMC) [8]) or variational approximations (e.g. Automatic Differentiation Variational Inference (ADVI) [9]). Whereas the latter are biased and underestimate uncertainty, the former methods may be exceedingly slow depending on the target distribution. For such reason, over the recent years, there has been an increasing interest in developing more efficient posterior approximations [10, 11, 12] and inference engines that aim to be the most general and flexible possible, so they can be used easily for any probabilistic model written as a program [13, 14].

It is well known that the performance of a sampling method depends on the parameters used [15]. In this work, we propose a framework to automatically adapt the shape of the posterior and also tune the parameters of a posterior sampler with the aim of boosting Bayesian inference efficiency in probabilistic programs. Our framework can be regarded as a principled way to enhance the flexibility of the variational posterior approximation, yet can be seen also as a procedure to tune the parameters of an MCMC sampler.

Our contributions can be summarised as follows:

- A new flexible and unbiased variational approximation to the posterior, which consists of improving an initial variational approximation with a stochastic process.
- An alternative ELBO function objective formulation, which is a variant of the original one when this new variational approximation is adopted.

- A specialization to the case of Bayesian inference in state-space models.

### 1.1 Related work

The idea of preconditioning the posterior distribution to speed up the mixing time of an MCMC sampler has recently been explored in [16] and [17], where a reparameterization is learned before performing the sampling via HMC. Both papers extend seminal work of [18] by learning an efficient and expressive deep, non-linear transformation instead of a polynomial regression. However, they do not account for tuning the parameters of the sampler as we introduce in Section 3, where a fully, end to end differentiable sampling scheme is proposed.

The work of [19] introduced a general framework for constructing more flexible variational distributions, called normalizing flows. These transformations are one of the main techniques to improve the flexibility of current VI approaches and have recently pervaded the literature of approximate Bayesian inference with current developments such as continuous-time normalizing flows [20] which extend an initial simple variational posterior with a discretization of Langevin dynamics. However, they require a generative adversarial network (GAN) [21] to learn the posterior, which can be unstable in high-dimensional spaces. We overcome this issue with the novel formulation stated in Section 3. Our framework is also compatible with different optimizers, not only those derived from Langevin dynamics. Other recent proposals to create more flexible variational posteriors are based on implicit approaches, which typically require a GAN [22] or implicit schema such as UIVI [23] or SIVI [24]. Our variational approximation is also implicit, but we use a sampling algorithm to drive the evolution of the density, combined with a Dirac delta approximation to derive an efficient variational approximation as we report on the extensive experiments in the Section 5.

Our work is also related to the recent idea of amortization of samplers [25]. A common problem with these approaches is that they incur in an additional error, the amortization gap [26]. We alleviate this by evolving a set of particles  $z_i$  with a stochastic process in the latent space after learning a good initial distribution. Hence, the bias generated by the initial approximation is significantly reduced after several iterations of the process. A recent article related to our paper is [27], who define a compound distribution similar to our framework. However, we focus on an efficient approximation using the reverse KL divergence, the standard and well understood divergence used in variational inference, which allows for tuning sampler parameters and achieving competitive results.

## 2 Background

A probabilistic program defines a probabilistic model  $p(x, z)$  that factorizes as

$$p(x, z) = p(x|z) \prod_{i=1}^n p(z_i|z_{<i}),$$

where  $n$  is the number of latent variables. The previous notation is convenient since it resembles the structure of a generic probabilistic model to sample from  $p(x, z)$ :

$$\begin{aligned} z_1 &\sim p(z_1) \\ z_2 &\sim p(z_2|z_{<2}) = p(z_2|z_1) \\ &\dots \\ z_n &\sim p(z_n|z_{<n}) \\ x &\sim p(x|z) \\ \text{observe } &x, \end{aligned}$$

where we have  $n + 1$  sampling statements and then we can condition on some observed data. Note that the last factor  $p(x|z)$  could be also further factorized. This formulation is sufficiently flexible to describe numerous models typically used in the Machine Learning community, such as the Hidden Markov Model, whose joint probability can be expressed as

$$p(x, z) = p(x|z) \prod_{i=1}^{\tau} p(z_i|z_{i-1}) = \prod_{i=1}^{\tau} p(x_i|z_i)p(z_i|z_{i-1}),$$

for a sequence of  $\tau$  observations  $x \in \mathbb{R}^{\tau}$ , and  $z_i$  being the hidden state of the observed  $x_i$ .

Sampling from  $p(x, z)$  is tractable as it is just required to run the program forward. However, performing inferences of the form  $p(z|x)$  (or some marginal) can be cumbersome, specially in large-scale settings when the number of observations is huge, or the parameters lie in high-dimensional spaces. We next summarise fundamental approaches to deal with this issue.

### 2.1 Inference as sampling

HMC [8] is an effective sampling method for models whose probability is point-wise computable and differentiable. When scalability is an issue, [28] proposed a formulation of a continuous-time Markov process that converges to a target distribution  $p(z|x)$  with  $z \in \mathbb{R}^d$ . It is based on the Euler-Maruyama discretization of Langevin dynamics:

$$z_{t+1} \leftarrow z_t - \eta_t \nabla \log p(z_t, x) + \mathcal{N}(0, 2\eta_t I), \quad (1)$$

where  $\eta_t$  is the step size. The required gradient  $\nabla \log p(z_t, x)$  can be estimated using mini-batches of data. Several extensions of the original Langevin sampler have been proposed to increase the mixing speed, see for instance [29, 30, 31, 32].

## 2.2 Inference as optimization

Variational inference, [9], tackles the problem of approximating the posterior  $p(z|x)$  with a tractable parameterized distribution  $q_\phi(z|x)$ . The goal is to find parameters  $\phi$  so that the variational distribution (also referred to as the variational guide or variational approximation)  $q_\phi(z|x)$  is as close as possible to the actual posterior. Closeness is typically measured through Kullback-Leibler divergence  $KL(q||p)$ , which is reformulated into the ELBO, the objective to be optimized using stochastic gradient descent techniques:

$$\text{ELBO}(q) = \mathbb{E}_{q_\phi(z|x)} [\log p(x, z) - \log q_\phi(z|x)]. \quad (2)$$

Typically, a deep, non-linear model conditioned on observation  $x$  defines the mean and covariance matrix of a Gaussian distribution  $q_\phi(z|x) \sim \mathcal{N}(\mu_\phi(x), \sigma_\phi(x))$ , to allow for greater flexibility.

## 3 The Variationally Inferred Sampling (VIS) framework

In standard VI, the variational approximation  $q_\phi(z|x)$  is analytically tractable. It is typically chosen as a factorized Gaussian distribution as described in Section 2.2. We propose to use a more flexible approximating posterior by embedding a sampler through:

$$q_{\phi,\eta}(z|x) = \int Q_{\eta,T}(z|z_0)q_{0,\phi}(z_0|x)dz_0, \quad (3)$$

where  $q_{0,\phi}(z|x)$  is the initial and tractable density (i.e., the starting state for the sampler). We will refer to  $q_{\phi,\eta}(z|x)$  as the refined variational approximation. The conditional distribution  $Q_{\eta,T}(z|z_0)$  refers to a stochastic process parameterized by  $\eta$  used to evolve the original density  $q_{0,\phi}(z|x)$  and achieve greater flexibility. In the following subsections we describe particular forms of  $Q_{\eta,T}(z|z_0)$ . When  $T = 0$ , no refinement steps are performed, so the refined variational approximation coincides with the original variational approximation,  $q_{\phi,\eta}(z|x) = q_{0,\phi}(z|x)$ . As  $T$  increases, the variational approximation will be closer to the exact posterior, provided that  $Q_{\eta,T}$  is a valid MCMC sampler. Next, instead of optimizing the ELBO, a refined ELBO is maximized,

$$\text{rELBO}(q) = \mathbb{E}_{q_{\phi,\eta}(z|x)} [\log p(x, z) - \log q_{\phi,\eta}(z|x)] \quad (4)$$

to optimize the divergence  $KL(q_{\phi,\eta}(z|x)||p(z|x))$ . The first term of the rELBO only requires sampling from  $q_{\phi,\eta}(z|x)$ ; however the second term, the entropy  $-\mathbb{E}_{q_{\phi,\eta}(z|x)} [\log q_{\phi,\eta}(z|x)]$  requires also evaluating the evolving, implicit density. Depending on the conditional distribution  $Q_{\eta,T}(z|z_0)$ , the integral (3) may be analytically tractable or not. We propose a set of effective guidelines for the rELBO optimization:

1. Consider the evolved density  $q_{\phi,\eta}(z|x)$  as a finite mixture of Dirac Deltas (i.e. we approximate the density using a finite set of particles), so the previous entropy is zero. In more detail, we sample  $z^1, \dots, z^K \sim q_{\phi,\eta}(z|x)$ , and then use  $\tilde{q}_{\phi,\eta}(z|x) = \frac{1}{K} \sum_{i=1}^K \delta(z - z^i)$  as the variational approximation.
2. An hybrid approach, in which some integrals can be analytically computed and the others approximated by the Delta approximation. See Section 3.3 for a discussion on this in the state-space model setting.

Regarding  $Q_{\eta,T}(z|z_0)$ , we consider the following families of sampling algorithms.

### 3.1 Continuous latent variables

When the latent variables  $z$  are continuous ( $z \in \mathbb{R}^d$ ), we propose to evolve the original variational density  $q_{0,\phi}(z|x)$  through a stochastic diffusion process. In order to make it tractable, we discretize the Langevin dynamics using the Euler-Maruyama scheme, arriving at the stochastic gradient Langevin dynamics (SGLD) sampler.

We now follow the process  $Q_{\eta,T}(z|z_0)$  (representing  $T$  iterations of an MCMC sampler). As an example, we make it explicit for the SGLD sampler through

$$z_i = z_{i-1} + \eta \nabla \log p(x, z_{i-1}) + \xi_i,$$

where  $i$  iterates from 1 to  $T$  and, in this case, the only parameter of the SGLD sampler is the learning rate  $\eta$ . The noise for the SGLD is denoted  $\xi_i \sim \mathcal{N}(0, 2\eta I)$ . Note that for some models, the previous gradient  $\nabla \log p(x, z_i)$  is a linear function of  $z_i$ , so we can compute the exact distribution of  $q(z_{i+1})$  from the distribution of  $q(z_i)$ . In other cases, we resort to approximate the non-analytical terms using the Delta approximation described before. Figure 1 provides a graphical representation of the variational approximation. The initial variational distribution,  $q_{0,\phi}(z|x)$  is a Gaussian parameterized by a deep neural network (NN). Then,  $T$  iterations of a sampler  $Q$ , parameterized by  $\eta$ , are applied leading to the final distribution  $q_{\phi,\eta}$ .

An alternative may be given by ignoring the noise vector  $\xi$  [33], thus refining the initial variational approximation with just the stochastic gradient descent (SGD). For this particular case, one can instead define a slightly different variational approximation instead of the Dirac Delta approximation, by treating the gradient terms as points but keeping a Gaussian distribution as the variational distribution. Details are shown in Appendix (Supp. Material) A. Moreover, we can use

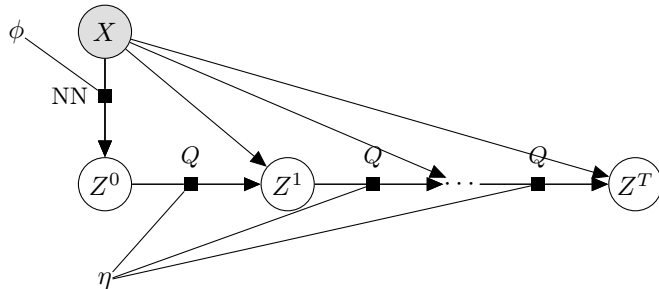


Figure 1: Probabilistic graph for the refined variational approximation.

Stein variational gradient descent (SVGD) [34] or a stochastic version [32] to apply repulsion between particles and promote a more extensive exploration of the latent space. The effect of using different samplers is left for future work.

### 3.2 Tuning sampler parameters

In standard VI, the variational approximation  $q(z|x; \phi)$  is parameterized by  $\phi$ . The parameters are learned using SGD or variants such as Adam [35], using the gradient  $\nabla_{\phi} \text{ELBO}(q)$ . Since we have shown how to embed a sampler inside the variational guide, it is also possible to compute a gradient of the objective with respect to the sampler parameters  $\eta$ . For instance, we can compute a gradient with respect to the learning rate  $\eta$  from the SGLD or SGD process from Section 3.1,  $\nabla_{\eta} \text{rELBO}(q)$ , to search for an optimal step size at every VI iteration. This is an additional step apart from using the gradient  $\nabla_{\phi} \text{rELBO}(q)$  which is used to learn a good initial sampling distribution.

### 3.3 State-space model specialization

The previous framework is particularly useful in large families of state-space models (and by extension, models that exhibit hierarchical and/or temporal structure), mainly through two complementary strategies: i) exact marginalization of some particular terms (i.e., Rao-Blackwellization [36] to reduce the variance); ii) exact computation in linear cases. Recall that a state-space model [37] can be expressed with the following probabilistic model, where the time-step  $t$  iterates from 1 to  $\tau$ :

$$\begin{aligned} z_{t+1} &\sim p(z_{t+1}|z_t, \theta_{tr}), \\ x_{t+1} &\sim p(x_{t+1}|z_{t+1}, \theta_{em}). \end{aligned}$$

This formulation subsumes many models used in Machine Learning such as Hidden Markov Models (HMMs) or Dynamic Linear Models (DLMs). It is often required to perform inference on the  $\theta := (\theta_{em}, \theta_{tr})$  parameters

from the transition and emission equations, respectively. We propose to use a variational distribution  $q(\theta)$ , which will be refined by any sampling method (as described in Section 3.1):

$$\theta \leftarrow \theta + \nabla_{\theta} \log p(x_{1:\tau}|z_{1:\tau}, \theta) + \xi. \quad (5)$$

Note that for a large class of models (including HMMs and DLMs) we can marginalize out  $z_{1:\tau}$  and have reduced variance iterating with:

$$\theta \leftarrow \theta + \nabla_{\theta} \log p(x_{1:\tau}|\theta) + \xi, \quad (6)$$

where the latent variables  $z_{1:\tau}$  have been marginalized out using the sum-product algorithm. For linear-Gaussian models we can also compute the exact form of the refined posterior, since all terms in Eq. 6 are linear wrt the latent variables  $\theta$ . However, inference in these linear models is exact by using conjugate distributions, so the proposed framework is more fit to the case of state-space models containing non-linear (or non-conjugate) components. For these families of models, we resort to use just a gradient estimator of the entropy or the Delta approximation in Section 3.1.

## 4 Analysis of VIS

In this Section we study in detail key properties of the proposed VIS framework.

### 4.1 Rewriting the ELBO

Performing variational inference with the refined variational approximation can be regarded as using the original variational guide while optimizing an alternative, tighter ELBO. Note that for a refined guide of the form  $q(z|z_0)q(z_0|x)$ , the objective function can be written as

$$\mathbb{E}_{q(z|z_0)q(z_0|x)} [\log p(x, z) - \log q(z|z_0) - \log q(z_0|x)].$$

However, using the Dirac Delta approximation for  $q(z|z_0)$  and noting that  $z = z_0 + \eta \nabla \log p(x, z_0)$  when using SGD with  $T = 1$ , we arrive at the modified objective:

$$\mathbb{E}_{q(z_0|x)} [\log p(x, z_0 + \eta \nabla \log p(x, z_0)) - \log q(z_0|x)]$$

which is equivalent to the refined ELBO introduced in (4). Since we are perturbing the latent variables in the steepest ascent direction, it is straightforward to show that, for moderate  $\eta$ ,

$$\text{ELBO}(q) \leq \text{rELBO}(q),$$

for the original variational guide  $q(z_0|x)$ . This reformulation of ELBO is also convenient since it provides a clear way of implementing our refined variational inference framework in any PPL supporting algorithmic differentiation.

## 4.2 Taylor expansion

From the result in subsection 4.1, we can further restrict to the case when the original variational approximation is also a Dirac point mass. Then, the original ELBO optimization resorts to the standard maximum likelihood estimation, i.e.,  $\max_z \log p(x, z)$ . Within the VIS framework, we optimize instead  $\max_z \log p(x, z + \Delta z)$ , where  $\Delta z$  is one iteration of the sampler, i.e.,  $\Delta z = \eta \nabla \log p(x, z)$  in the SGD case. For notational clarity we resort to the case  $T = 1$ , but a similar analysis can be straightforwardly done if more refinement steps are performed.

We may now perform a first-order Taylor expansion of the refined objective as

$$\log p(x, z + \Delta z) \approx \log p(x, z) + (\Delta z)^\top \nabla \log p(x, z).$$

Taking gradients of the first order approximation w.r.t. the latent variables  $z$  we arrive at

$$\nabla_z \log p(x, z) + \eta \nabla_z \log p(x, z)^\top \nabla_z^2 \log p(x, z),$$

where we have not computed the gradient through the  $\Delta z$  term. That is, the *refined gradient* can be deemed as the original gradient plus a second order correction. Instead of being modulated by a constant learning rate, this correction is adapted by the chosen sampler. In the experiments in Section 5.4 we show that this is beneficial for the optimization as it can take less iterations to achieve lower losses. By further taking gradients through the  $\Delta z$  term, we may tune the sampler parameters such as the learning rate as described in Section 3.2. Consequently, the next subsection describes both modes of differentiation.

## 4.3 Two modes of Automatic Differentiation for rELBO optimization

Here we describe how to implement two variants of the rELBO objective. First, we define a *stop gradient* operator<sup>1</sup>  $\perp$  that sets the gradient of its operand to zero, i.e.,  $\nabla_x \perp(x) = 0$  whereas in the forward pass it acts as the identity function, that is,  $\perp(x) = x$ . Then, the two variants of the rELBO objective are

$$\mathbb{E}_q [\log p(x, z + \Delta z) - \log q(z + \Delta z|x)] \quad (\text{Full AD})$$

and

$$\mathbb{E}_q [\log p(x, z + \perp(\Delta z)) - \log q(z + \perp(\Delta z)|x)]. \quad (\text{Fast AD})$$

The Full AD rELBO makes it possible to further compute a gradient wrt sampler parameters inside  $\Delta z$  at the cost of a slight increase in the computational burden. However, the Fast AD variant may be handy in multiple scenarios as we illustrate below.

<sup>1</sup>corresponds to `detach` in Pytorch or `stop_gradient` in tensorflow.

## 5 Experiments

We first detail the experiments. We emphasize that our framework permits rapid iterations over a large class of models (i.e., it is more automatic than, e.g., manually setting up a Gibbs sampler). Through the following experiments, we aim to shed light on the following questions:

- Q1** Is the increased computational complexity of computing gradients through sampling steps worth the flexibility gains?
- Q2** Is the proposed framework compatible with other structured inference techniques, such as the sum-product algorithm?
- Q3** Does the more flexible posterior approximated by VIS help in auxiliary tasks, such as decision making or classification?

Within the spirit of reproducible research, the code will be released at <https://github.com/vicgalle/vis>. The VIS framework was implemented using Pytorch [38], though we also release a notebook for the first experiment using Jax to highlight the simple implementation of the VIS framework.

### 5.1 Funnel density

As a preliminary experiment, we test the VIS framework on a synthetic yet complex target distribution. The target, bi-dimensional density is defined through:

$$\begin{aligned} z_1 &\sim \mathcal{N}(0, 1.35) \\ z_2 &\sim \mathcal{N}(0, \exp(z_1)). \end{aligned}$$

As a variational approximation we take the usual diagonal Gaussian distribution. For the VIS case, we consider to refine it for  $T = 1$  steps using SGLD. Results are shown in Figure 2. In the top, we show the trajectories of the lower bound for up to 50 iterations of variational optimization with Adam. It is clear that our refined version achieves a tighter bound. The middle and bottom figures present the contour curves of the learned variational approximations. The VIS variant is placed nearer to the mean of the true distribution and is more disperse than the original variational approximation, confirming the fact that the refinement step helps in attaining more flexible posterior approximations.

### 5.2 State-space Markov models

We test our variational approximation on two state-space models, one for discrete data and the other for continuous observations. All the experiments in this

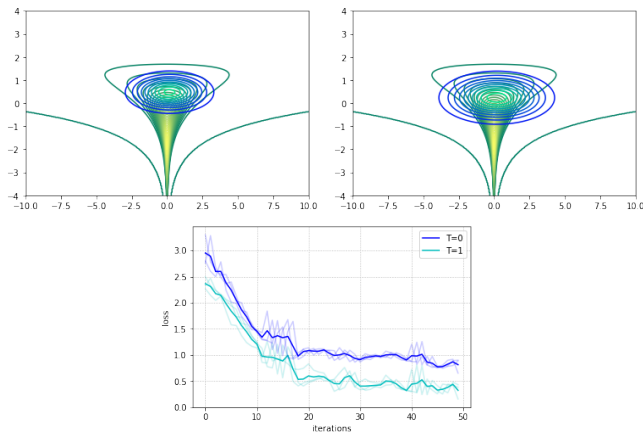


Figure 2: Bottom: evolution of the -ELBO loss objective through 50 iterations. Darker lines depict the mean along different seeds (lighter lines). Top left: contour curves (blue-turquoise) of the variational approximation with no refinement ( $T = 0$ ) at iteration 30 (loss of 1.011). Top right: contour curves (blue-turquoise) of the refined variational approximation ( $T = 1$ ) at iteration 30 (loss of 0.667). Green-yellow curves denote the target density.

subsection use the Fast AD version from Section 4.3 since it was not necessary to further tune the sampler parameters to have competitive results.

**Hidden Markov Model (HMM).** The model equations are given by

$$p(z_{1:\tau}, x_{1:\tau}, \theta) = \prod_{t=1}^{\tau} p(x_t | z_t, \theta_{em}) p(x_t | x_{t-1}, \theta_{tr}) p(\theta),$$

where each conditional is a Categorical distribution which takes 5 different classes and the prior  $p(\theta) = p(\theta_{em})p(\theta_{tr})$  are two Dirichlet distributions that sample the emission and transition probabilities, respectively. We perform inference on the parameters  $\theta$ .

**Dynamic Linear Model (DLM).** The model equations are the same as in the HMM case, though the conditional distributions are now Gaussian and the parameters  $\theta$  refer to the emission and transition variances. As before, we perform inference over  $\theta$ .

The full model implementations can be checked in Appendix (Supp. Material) B.1, based on `funsor`<sup>2</sup>, a PPL on top of the Pytorch autodiff framework. For each model, we generate a synthetic dataset, and use the refined variational approximation with  $T = 0, 1, 2$ . As the original variational approximation to the parameters  $\theta$  we use a Dirac Delta. Performing VI with

this approximation corresponds to MAP estimation using the Kalman filter in the DLM case [39] and the Baum-Welch algorithm in the HMM case [6], since we marginalize out the latent variables  $z_{1:\tau}$ . Model details are given in Appendix (Supp. Material) B.1.1. Figure 3 shows the results. The first row reports the experiments related to the HMM; the second one to the DLM. While in all graphs we report the evolution of the loglikelihood during inference, in the first column we report the number of rELBO iterations, whereas in the second column we measure wall-clock time as the optimization takes place. We confirm that VIS ( $T > 0$ ) achieve better results than regular optimization with VI ( $T = 0$ ) for a similar amount of time.

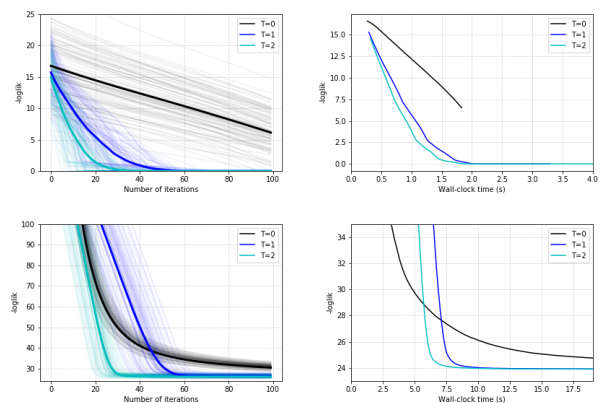


Figure 3: Results of rELBO optimization for state-space models. Top left (HMM): -loglikelihood against number of rELBO gradient iterations. Top right (HMM): -loglikelihood against wall-clock time. Bottom left (DLM): -loglikelihood against number of rELBO gradient iterations. Bottom right (DLM): -loglikelihood against number of rELBO gradient iterations

## 5.2.1 Prediction tasks in a HMM

With the aim of assessing whether rELBO optimization helps in attaining better auxiliary scores, we also report results on a prediction task. We generate a synthetic time series of alternating 0 and 1 for  $\tau = 105$  timesteps. We train the HMM model from before on the first 100 points, and report in Table 1 the accuracy of the predictive distribution  $p(y_t)$  averaged over the last 5 time-steps. We also report the predictive entropy since it helps in assessing the confidence of the model in its forecast and is a strictly proper scoring rule [40]. To guarantee the same computational budget time and a fair comparison, the model without refining is run with 50 epochs, whereas the model with refinement is run for 20 epochs. We see that the refined model achieves higher accuracy than its counterpart; in addition it is correctly more confident in its predictions.

<sup>2</sup><https://github.com/pyro-ppl/funsor/>

Table 1: Prediction metrics for the HMM.

	$T = 0$	$T = 1$
accuracy	0.40	<b>0.84</b>
predictive entropy	1.414	<b>1.056</b>
logarithmic score	-1.044	<b>-0.682</b>

### 5.2.2 Prediction task in a DLM

We now test the VIS framework on the Mauna Loa monthly  $CO_2$  time series data [41]. As the training set, we take the first 10 years, and we evaluate over the next 2 years. We use a DLM composed of a local linear trend plus a seasonality block of periodicity 12. Full model specification can be checked in Appendix (Supp. Material) B.1. As a preprocessing step, we standardize the time series to zero mean and unitary deviation. To guarantee the same computational budget time, the model without refining is run for 10 epochs, whereas the model with refinement is run for 4 epochs. We report mean absolute error (MAE) and predictive entropy in Table 2. In addition, we compute the interval score as defined in [40], a strictly proper scoring rule. As can be seen, for similar wall-clock times, the refined model not only achieves lower MAE, but also its predictive intervals are narrower than the non-refined counterpart.

Table 2: Prediction metrics for the DLM.

	$T = 0$	$T = 1$
MAE	0.270	<b>0.239</b>
predictive entropy	2.537	<b>2.401</b>
interval score ( $\alpha = 0.05$ )	15.247	<b>13.461</b>

### 5.3 Variational Autoencoder

The third batch of experiments aims to check whether the VIS framework is competitive with respect to other algorithms from the recent literature. To this end, we test our approach in a Variational Autoencoder (VAE) model [5]. Performing efficient and flexible inference in a VAE is useful since it is the building block of more complex models and tasks [42, 43]. The VAE defines a conditional distribution  $p_\theta(x|z)$ , generating an observation  $x$  from a latent variable  $z$ . For this task, we are interested in modelling two  $28 \times 28$  image distributions, MNIST and fashion-MNIST. To perform inference (learn parameters  $\theta$ ) the VAE introduces a variational approximation  $q_\phi(z|x)$ . In the standard setting, this distribution is Gaussian; we instead use the refined variational approximation comparing various values of  $T$ . We also use the Full AD variant from Section 4.3.

As experimental setup, we reproduce the setting from [23]. As model  $p_\theta(x|z)$ , we use a factorized Bernoulli dis-

tribution parameterized with a two layer feed-forward network with 200 units in each layer and relu activation, except for the final sigmoid activation. As variational approximation  $q_\phi(z|x)$ , we use a Gaussian whose mean and (diagonal) covariance matrix are parameterized by two separate neural networks with the same structure as the previous one, except the sigmoid activation for the mean and a softplus activation for the covariance matrix.

 Table 3: Test log-likelihood on binarized MNIST and fMNIST. VIS- $X$ - $Y$  denotes  $T = X$  refinement iterations during training and  $T = Y$  refinement iterations during testing.

Method	MNIST	fMNIST
	Results from [23]	
UIVI	-94.09	-110.72
SIVI	-97.77	-121.53
VAE	-98.29	-126.73
	Results from [27]	
VCD	-95.86	-117.65
HMC-DLGM	-96.23	-117.74
	This paper	
VIS-5-10	<b>-73.85 <math>\pm</math> 0.79</b>	<b>-97.53 <math>\pm</math> 0.73</b>
VIS-0-10	-96.16 $\pm$ 0.17	-120.53 $\pm$ 0.59
VAE (VIS-0-0)	-100.91 $\pm$ 0.16	-125.57 $\pm$ 0.63

Results are reported in Table 3. To guarantee a fair comparison, we trained the VIS-5-10 variant for 10 epochs, whereas all the other variants were trained for 15 epochs (fMNIST) or 20 epochs (MNIST), so that the VAE performance is comparable to the one reported in [23]. Although VIS is trained for less epochs, by increasing the number of MCMC iterations  $T$ , we dramatically improve on test log-likelihood. In terms of computational complexity, the average time per epoch using  $T = 5$  is 10.46 s, whereas with no refinement ( $T = 0$ ) is 6.10 s (hence our decision to train the refined variant for less epochs): a moderate increase in computing time may be worth the dramatic increase in log-likelihood while not introducing new parameters in the model, except for the learning rate  $\eta$ . We also show the results from the contrastive divergence approach from [27] and the HMC variant from [44], showing that our framework can outperform those approaches in similar experimental settings. Finally, as a visual inspection of the quality of reconstruction from the VAE trained with the VIS framework, Figure 4 displays ten random samples of reconstructed digit images.

### 5.4 Variational Autoencoder as a deep Bayes Classifier

With the final experiments we show that the VIS framework can deal with more general probabilistic graphical

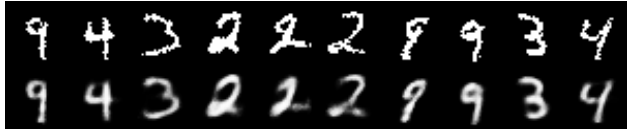


Figure 4: Top row: original images. Bottom row: reconstructed images using VIS-5-10 at 10 epochs.

models. Influence diagrams [45] are one of the most familiar representations of a decision analysis problem. There is a long history on bridging the gap between influence diagrams and probabilistic graphical models (see [46], for instance), so developing better tools for Bayesian inference can be automatically used to solve influence diagrams.

We showcase the flexibility of the proposed scheme to solve inference problems in an experiment with a classification task in a high-dimensional setting. As dataset, the MNIST [47] handwritten digit classification task is chosen, in which grey-scale  $28 \times 28$  images have to be classified in one of the ten classes  $\mathcal{Y} = \{0, 1, \dots, 9\}$ . More concretely, we extend the VAE model to condition it on a discrete variable  $y$ , leading to the conditional VAE (cVAE). A cVAE defines a decoder distribution  $p_\theta(x|z, y)$  on an input space  $x \in \mathbb{R}^D$  given class label  $y \in \mathcal{Y}$  and latent variable  $z \in \mathbb{R}^d$ . To perform inference, a variational posterior is learned as an encoder  $q_\phi(z|x, y)$  from a prior  $p(z) \sim \mathcal{N}(0, I)$ . Leveraging the conditional structure on  $y$ , we use the generative model as a classifier using Bayes rule:

$$\begin{aligned} p(y|x) &\propto p(y)p(x|y) = p(y) \int p_\theta(x|z, y)q_\phi(z|x, y)dz \\ &\approx \frac{1}{K} \sum_{k=1}^K p_\theta(x|z^{(k)}, y)p(y) \end{aligned} \quad (7)$$

where we use  $K$  Monte Carlo samples  $z^{(k)} \sim q_\phi(z|x, y)$ . In the experiments we set  $K = 5$ . Given a test sample  $x$ , the label  $\hat{y}$  with highest probability  $p(y|x)$  is predicted. Figure 6 in Appendix (Supp. Material) depicts the corresponding influence diagram. Additional details regarding the model architecture and hyperparameters can be found in Appendix (Supp. Material) B.

For comparison purposes, we perform various experiments changing  $T$  for the transition distribution  $Q_{\eta, T}$  in the refined variational approximation. Results are in Table 4. We report the test accuracy achieved at the end of training. Note we are comparing different values of  $T$  depending on being on the training or testing phases (in the latter, where the model and variational parameters are kept frozen). The model with  $T_{tr} = 5$  was trained for 10 epochs, whereas the other settings for 15 epochs, in order to give all settings similar training times. Results are averaged from 3 runs with differ-

Table 4: Results on digit classification task using a deep Bayes classifier.

$T_{tr}$	$T_{te}$	Acc. (test)
0	0	$96.5 \pm 0.5$ %
0	10	$97.7 \pm 0.7$ %
5	10	<b><math>99.8 \pm 0.2</math> %</b>

ent random seeds. From the results it is clear that the effect of using the refined variational approximation (the cases when  $T > 0$ ) is crucially beneficial to achieve higher accuracy. The effect of learning a good initial distribution and inner learning rate by using the gradients  $\nabla_{\phi} \text{rELBO}(q)$  and  $\nabla_{\eta} \text{rELBO}(q)$  has a highly positive impact in the accuracy obtained.

On a final note, we have not included the case when only using a SGD or SGLD sampler (i.e., without learning an initial distribution  $q_{0, \phi}(z|x)$ ) since the results were much worse than the ones in Table 4, for a comparable computational budget. This strongly suggests that for inference in high-dimensional, continuous latent spaces, learning a good initial distribution through VIS can dramatically accelerate mixing time.

## 6 Conclusion

We have proposed a flexible and efficient framework to perform inference in probabilistic programs. We have shown that the scheme can be easily implemented under the probabilistic programming paradigm and used to efficiently perform inference in a wide class of models: state space time series, variational autoencoders and influence diagrams, defined with continuous, high-dimensional distributions.

Our framework can be seen as a general way of tuning MCMC sampler parameters, adapting the initial distributions and the learning rate, Section 5. Key to the success and applicability of the VIS framework is the Dirac Delta approximation of the refined variational approximation, which is computationally cheap but convenient. Better estimates of the refined density and its gradient may be a fruitful line of research, such as the spectral estimator from [48]. Of independent interest to deal with the implicit variational density, it may be worthwhile to consider optimizing the Fenchel dual of the KL divergence, as done recently in [49]. However, this requires the use of an auxiliary neural network, which is a large computational price to pay compared with our lightweight particle approximation.

**Acknowledgments** VG acknowledges support from grant FPU16-05034. DRI is grateful to the MINECO MTM2014-56949-C3-1-R project and the AXA-ICMAT Chair in Adversarial Risk Analysis. All authors ac-

knowledge support from the Severo Ochoa Excellence Programme SEV-2015-0554. This material was based upon work partially supported by the National Science Foundation under Grant DMS-1638521 to the Statistical and Applied Mathematical Sciences Institute. Any opinions, findings, and conclusions or recommendations expressed in this material are those of the author(s) and do not necessarily reflect the views of the National Science Foundation.

## References

- [1] David J Lunn, Andrew Thomas, Nicky Best, and David Spiegelhalter. Winbugs-a bayesian modelling framework: concepts, structure, and extensibility. *Statistics and computing*, 10(4):325–337, 2000.
- [2] Bob Carpenter, Andrew Gelman, Matthew D Hoffman, Daniel Lee, Ben Goodrich, Michael Betancourt, Marcus Brubaker, Jiqiang Guo, Peter Li, and Allen Riddell. Stan: A probabilistic programming language. *Journal of statistical software*, 76(1), 2017.
- [3] Dustin Tran, Matthew W Hoffman, Dave Moore, Christopher Suter, Srinivas Vasudevan, and Alexey Radul. Simple, distributed, and accelerated probabilistic programming. In *Advances in Neural Information Processing Systems*, pages 7609–7620, 2018.
- [4] Eli Bingham, Jonathan P Chen, Martin Jankowiak, Fritz Obermeyer, Neeraj Pradhan, Theofanis Karaletsos, Rohit Singh, Paul Szerlip, Paul Horsfall, and Noah D Goodman. Pyro: Deep universal probabilistic programming. *arXiv preprint arXiv:1810.09538*, 2018.
- [5] Diederik P Kingma and Max Welling. Auto-encoding variational bayes. *arXiv preprint arXiv:1312.6114*, 2013.
- [6] Lawrence R Rabiner. A tutorial on hidden markov models and selected applications in speech recognition. *Proceedings of the IEEE*, 77(2):257–286, 1989.
- [7] Christophe Andrieu, Arnaud Doucet, and Roman Holenstein. Particle Markov chain monte carlo methods. *Journal of the Royal Statistical Society: Series B (Statistical Methodology)*, 72(3):269–342, 2010.
- [8] Radford M Neal et al. Mcmc using hamiltonian dynamics. *Handbook of Markov Chain Monte Carlo*, 2(11):2, 2011.
- [9] Alp Kucukelbir, Dustin Tran, Rajesh Ranganath, Andrew Gelman, and David M Blei. Automatic differentiation variational inference. *The Journal of Machine Learning Research*, 18(1):430–474, 2017.
- [10] Eric Nalisnick, Lars Hertel, and Padhraic Smyth. Approximate inference for deep latent gaussian mixtures. 2016.
- [11] Tim Salimans, Diederik Kingma, and Max Welling. Markov chain monte carlo and variational inference: Bridging the gap. In *International Conference on Machine Learning*, pages 1218–1226, 2015.
- [12] Dustin Tran, Rajesh Ranganath, and David M Blei. The variational gaussian process. *arXiv preprint arXiv:1511.06499*, 2015.
- [13] Frank Wood, Jan Willem Meent, and Vikash Mansinghka. A new approach to probabilistic programming inference. In *Artificial Intelligence and Statistics*, pages 1024–1032, 2014.
- [14] Hong Ge, Kai Xu, and Zoubin Ghahramani. Turing: a language for flexible probabilistic inference. In *International Conference on Artificial Intelligence and Statistics, AISTATS 2018, 9-11 April 2018, Playa Blanca, Lanzarote, Canary Islands, Spain*, pages 1682–1690, 2018.
- [15] Omiros Papaspiliopoulos, Gareth O Roberts, and Martin Sködl. A general framework for the parametrization of hierarchical models. *Statistical Science*, pages 59–73, 2007.
- [16] Matthew D Hoffman, Pavel Sountsov, Joshua Dillon, Ian Langmore, Dustin Tran, and Srinivas Vasudevan. Neutralizing bad geometry in hamiltonian monte carlo using neural transport. 2018.
- [17] Shuo-Hui Li and Lei Wang. Neural network renormalization group. *Phys. Rev. Lett.*, 121:260601, Dec 2018.
- [18] Matthew Parno and Youssef Marzouk. Transport map accelerated markov chain monte carlo. *arXiv preprint arXiv:1412.5492*, 2014.
- [19] Danilo Rezende and Shakir Mohamed. Variational inference with normalizing flows. In *International Conference on Machine Learning*, pages 1530–1538, 2015.
- [20] Changyou Chen, Chunyuan Li, Liqun Chen, Wenlin Wang, Yunchen Pu, and Lawrence Carin. Continuous-time flows for efficient inference and density estimation, 2018.

- [21] Ian Goodfellow, Jean Pouget-Abadie, Mehdi Mirza, Bing Xu, David Warde-Farley, Sherjil Ozair, Aaron Courville, and Yoshua Bengio. Generative adversarial nets. In *Advances in neural information processing systems*, pages 2672–2680, 2014.
- [22] Ferenc Huszár. Variational inference using implicit distributions. *arXiv preprint arXiv:1702.08235*, 2017.
- [23] Michalis K Titsias and Francisco Ruiz. Unbiased implicit variational inference. In *The 22nd International Conference on Artificial Intelligence and Statistics*, pages 167–176, 2019.
- [24] Mingzhang Yin and Mingyuan Zhou. Semi-implicit variational inference. *arXiv preprint arXiv:1805.11183*, 2018.
- [25] Yihao Feng, Dilin Wang, and Qiang Liu. Learning to draw samples with amortized stein variational gradient descent. *arXiv preprint arXiv:1707.06626*, 2017.
- [26] Chris Cremer, Xuechen Li, and David Duvenaud. Inference suboptimality in variational autoencoders. *arXiv preprint arXiv:1801.03558*, 2018.
- [27] Francisco Ruiz and Michalis Titsias. A contrastive divergence for combining variational inference and MCMC. In Kamalika Chaudhuri and Ruslan Salakhutdinov, editors, *Proceedings of the 36th International Conference on Machine Learning*, volume 97 of *Proceedings of Machine Learning Research*, pages 5537–5545, Long Beach, California, USA, 09–15 Jun 2019. PMLR.
- [28] Max Welling and Yee W Teh. Bayesian learning via stochastic gradient langevin dynamics. In *Proceedings of the 28th International Conference on Machine Learning (ICML-11)*, pages 681–688, 2011.
- [29] Chunyuan Li, Changyou Chen, David Carlson, and Lawrence Carin. Preconditioned stochastic gradient langevin dynamics for deep neural networks. In *Thirtieth AAAI Conference on Artificial Intelligence*, 2016.
- [30] Chunyuan Li, Changyou Chen, Kai Fan, and Lawrence Carin. High-order stochastic gradient thermostats for bayesian learning of deep models. In *Thirtieth AAAI Conference on Artificial Intelligence*, 2016.
- [31] Gabriele Abbati, Alessandra Tosi, Michael Osborne, and Seth Flaxman. Adageo: Adaptive geometric learning for optimization and sampling. In *International Conference on Artificial Intelligence and Statistics*, pages 226–234, 2018.
- [32] Victor Gallego and David Rios Insua. Stochastic gradient mcmc with repulsive forces. *arXiv preprint arXiv:1812.00071*, 2018.
- [33] Stephan Mandt, Matthew D Hoffman, and David M Blei. Stochastic gradient descent as approximate bayesian inference. *The Journal of Machine Learning Research*, 18(1):4873–4907, 2017.
- [34] Qiang Liu and Dilin Wang. Stein variational gradient descent: A general purpose bayesian inference algorithm. In *Advances In Neural Information Processing Systems*, pages 2378–2386, 2016.
- [35] Diederik P Kingma and Jimmy Ba. Adam: A method for stochastic optimization. *arXiv preprint arXiv:1412.6980*, 2014.
- [36] Lawrence Murray, Daniel Lundén, Jan Kudlicka, David Broman, and Thomas B Schön. Delayed sampling and automatic rao-blackwellization of probabilistic programs. In *International Conference on Artificial Intelligence and Statistics (AISTATS)*, 2018.
- [37] James D Hamilton. State-space models. *Handbook of econometrics*, 4:3039–3080, 1994.
- [38] Adam Paszke, Sam Gross, Soumith Chintala, Gregory Chanan, Edward Yang, Zachary DeVito, Zeming Lin, Alban Desmaison, Luca Antiga, and Adam Lerer. Automatic differentiation in pytorch. 2017.
- [39] Paul Zarchan and Howard Musoff. *Fundamentals of Kalman filtering: a practical approach*. American Institute of Aeronautics and Astronautics, Inc., 2013.
- [40] Tilmann Gneiting and Adrian E Raftery. Strictly proper scoring rules, prediction, and estimation. *Journal of the American Statistical Association*, 102(477):359–378, 2007.
- [41] Charles D Keeling. Atmospheric carbon dioxide record from mauna loa. 2005.
- [42] Liqun Chen, Shuyang Dai, Yunchen Pu, Erjin Zhou, Chunyuan Li, Qinliang Su, Changyou Chen, and Lawrence Carin. Symmetric variational autoencoder and connections to adversarial learning. In *International Conference on Artificial Intelligence and Statistics*, pages 661–669, 2018.
- [43] Diane Bouchacourt, Ryota Tomioka, and Sebastian Nowozin. Multi-level variational autoencoder: Learning disentangled representations from grouped observations. In *Thirty-Second AAAI Conference on Artificial Intelligence*, 2018.

- [44] Matthew D. Hoffman. Learning deep latent Gaussian models with Markov chain Monte Carlo. In Doina Precup and Yee Whye Teh, editors, *Proceedings of the 34th International Conference on Machine Learning*, volume 70 of *Proceedings of Machine Learning Research*, pages 1510–1519, International Convention Centre, Sydney, Australia, 06–11 Aug 2017. PMLR.
- [45] Ronald A Howard and James E Matheson. Influence diagrams. *Decision Analysis*, 2(3):127–143, 2005.
- [46] Ross D. Shachter. Probabilistic inference and influence diagrams. *Operations Research*, 36(4):589–604, 1988.
- [47] Yann LeCun, Léon Bottou, Yoshua Bengio, Patrick Haffner, et al. Gradient-based learning applied to document recognition. *Proceedings of the IEEE*, 86(11):2278–2324, 1998.
- [48] Jiaxin Shi, Shengyang Sun, and Jun Zhu. A spectral approach to gradient estimation for implicit distributions. In *International Conference on Machine Learning*, pages 4651–4660, 2018.
- [49] Le Fang, Chunyuan Li, Jianfeng Gao, Wen Dong, and Changyou Chen. Implicit deep latent variable models for text generation, 2019.

## A Alternative variational approximation

We introduced the VIS posterior as

$$q_{\phi,\eta}(z|x) = \int Q_{\eta,T}(z|z_0)q_{0,\phi}(z_0|x)dz_0.$$

In order to compute the ELBO, we sample  $z^1, \dots, z^K \sim q_{\phi,\eta}(z|x)$ , and then use  $\tilde{q}_{\phi,\eta}(z|x) = \frac{1}{K} \sum_{i=1}^K \delta(z - z^i)$  as the variational approximation. Though cheap to compute and competitive in our experiments, there are settings where it could be helpful to have a posterior approximation that places density over the whole latent space. For the particular case of using SGD as the inner kernel, we have

$$\begin{aligned} z_0 &\sim q_{0,\phi}(z_0|x) = \mathcal{N}(z_0|\mu_\phi(x), \sigma_\phi(x)) \\ z_i &= z_{i-1} + \eta \nabla \log p(x, z_{i-1}), \quad i = 1, \dots, T. \end{aligned}$$

By treating the gradient terms as points, we have that the refined variational approximation can be computed as

$$q_{\phi,\eta}(z|x) = \mathcal{N}(z|z_T, \sigma_\phi(x)).$$

Note that there is an implicit dependence on  $\eta$  through  $z_T$ .

## B Experiment details

### B.1 State-space models

#### B.1.1 Initial experiments

For the HMM, both the emission and transition probabilities are Categorical distributions, taking values in the domain  $\{0, 1, 2, 3, 4\}$ .

The equations of the DLM are given by

$$\begin{aligned} z_{t+1} &\sim \mathcal{N}(0.5z_t + 1.0, \sigma_{tr}) \\ x_t &\sim \mathcal{N}(3.0z_t + 0.5, \sigma_{em}). \end{aligned}$$

with  $z_0 = 0.0$ .

#### B.1.2 Prediction task in a DLM

The DLM model is comprised of a linear trend component plus a seasonal block of period 12. The trend is specified as

$$\begin{aligned} x_t &= \mu_t + \epsilon_t & \epsilon_t &\sim \mathcal{N}(0, \sigma_{obs}) \\ \mu_t &= \mu_{t-1} + \delta_{t-1} + \epsilon'_t & \epsilon'_t &\sim \mathcal{N}(0, \sigma_{level}) \\ \delta_t &= \delta_{t-1} + \epsilon''_t & \epsilon''_t &\sim \mathcal{N}(0, \sigma_{slope}). \end{aligned}$$

With respect to the seasonal component, the main idea is to *cycle the state*: suppose  $\theta_t \in \mathbb{R}^p$ , with  $p$  being the

seasonal period. Then, at each timestep, the model focuses on the first component of the state vector:

$$(\alpha_1, \alpha_2, \dots, \alpha_p) \xrightarrow{\text{next period}} (\alpha_2, \alpha_3, \dots, \alpha_p, \alpha_1).$$

Thus, we can specify the seasonal component via:

$$\begin{aligned} x_t &= F\theta_t + v_t \\ \theta_t &= G\theta_{t-1} + w_t \end{aligned}$$

where  $F$  is a  $p$ -dimensional vector and  $G$  is a  $p \times p$  matrix such that

$$G = \begin{bmatrix} 0 & 0 & \dots & 0 & 1 \\ 1 & 0 & & 0 & 0 \\ 0 & 1 & & 0 & 0 \\ & & \ddots & & \\ 0 & 0 & & 1 & 0 \end{bmatrix}$$

and  $F = (1, 0, \dots, 0, 0)$ .

## B.2 VAE

### B.2.1 Model details

```
class VAE(nn.Module):
    def __init__(self):
        super(VAE, self).__init__()

        self.z_d = 10
        self.h_d = 200
        self.x_d = 28*28

        self.fc1_mu = nn.Linear(self.x_d, self.h_d)
        self.fc1_cov = nn.Linear(self.x_d, self.h_d)
        self.fc12_mu = nn.Linear(self.h_d, self.h_d)
        self.fc12_cov = nn.Linear(self.h_d, self.h_d)
        self.fc2_mu = nn.Linear(self.h_d, self.z_d)
        self.fc2_cov = nn.Linear(self.h_d, self.z_d)

        self.fc3 = nn.Linear(self.z_d, self.h_d)
        self.fc32 = nn.Linear(self.h_d, self.h_d)
        self.fc4 = nn.Linear(self.h_d, self.x_d)

    def encode(self, x):
        h1_mu = F.relu(self.fc1_mu(x))
        h1_cov = F.relu(self.fc1_cov(x))
        h1_mu = F.relu(self.fc12_mu(h1_mu))
        h1_cov = F.relu(self.fc12_cov(h1_cov))
        # we work in the logvar-domain
        return self.fc2_mu(h1_mu),
        torch.log(F.softplus(self.fc2_cov(h1_cov)))

    def decode(self, z):
        h3 = F.relu(self.fc3(z))
        h3 = F.relu(self.fc32(h3))
        return torch.sigmoid(self.fc4(h3))
```

Figure 5: Model architecture for the cVAE.

The VAE model is implemented with PyTorch [38]. The prior distribution  $p(z)$  for the latent variables  $z \in \mathbb{R}^{10}$  is a standard factorized Gaussian. The decoder distribution  $p_\theta(x|z)$  and the encoder distribution (initial variational approximation)  $q_{0,\phi}(z|x)$  are parameterized by two feed-forward neural networks whose details can be checked in Figure 5.

### B.2.2 Hyperparameter settings

The optimizer Adam is used in all experiments, with a learning rate  $\lambda = 0.001$ . We also set  $\eta = 0.001$ . We train for 15 epochs (fMNIST) and 20 epochs (MNIST), in order to achieve similar performance to the explicit VAE case in [23]. For the VIS-5-10 setting, we train for only 10 epochs, to allow for a fair computational comparison (similar computing times).

### B.3 CVAE

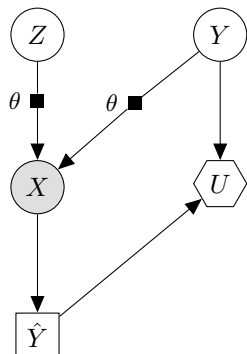


Figure 6: Influence Diagram for the deep Bayes classifier.

### B.3.1 Model details

```

class cVAE(nn.Module):
    def __init__(self):
        super(cVAE, self).__init__()

        self.z_d = 10
        self.h_d = 200
        self.x_d = 28*28
        num_classes = 10

        self.fc1_mu = nn.Linear(self.x_d + num_classes, self.h_d)
        self.fc1_cov = nn.Linear(self.x_d + num_classes, self.h_d)
        self.fc12_mu = nn.Linear(self.h_d, self.h_d)
        self.fc12_cov = nn.Linear(self.h_d, self.h_d)
        self.fc2_mu = nn.Linear(self.h_d, self.z_d)
        self.fc2_cov = nn.Linear(self.h_d, self.z_d)

        self.fc3 = nn.Linear(self.z_d + num_classes, self.h_d)
        self.fc32 = nn.Linear(self.h_d, self.h_d)
        self.fc4 = nn.Linear(self.h_d, self.x_d)

    def encode(self, x, y):
        h1_mu = F.relu(self.fc1_mu(torch.cat([x, y], dim=-1)))
        h1_cov = F.relu(self.fc1_cov(torch.cat([x, y], dim=-1)))
        h1_mu = F.relu(self.fc12_mu(h1_mu))
        h1_cov = F.relu(self.fc12_cov(h1_cov))
        # we work in the logvar-domain
        return self.fc2_mu(h1_mu),
            torch.log(F.softplus(self.fc2_cov(h1_cov)))

    def decode(self, z, y):
        h3 = F.relu(self.fc3(torch.cat([z, y], dim=-1)))
        h3 = F.relu(self.fc32(h3))
        return torch.sigmoid(self.fc4(h3))
  
```

Figure 7: Model architecture for the cVAE.

The prior distribution  $p(z)$  for the latent variables  $z \in \mathbb{R}^{10}$  is a standard factorized Gaussian. The decoder distribution  $p_{\theta}(x|y, z)$  and the encoder distribution (initial variational approximation)  $q_{0,\phi}(z|x, y)$  are parameterized by two feed-forward neural networks whose details can be checked in Figure 7. The integral (7) is approximated with 1 MC sample from the variational approximation in all experimental settings.

### B.3.2 Hyperparameter settings

The optimizer Adam is used in all the experiments, with a learning rate  $\lambda = 0.01$ . We set the initial  $\eta = 5e - 5$ .

The cVAE model is implemented with PyTorch [38].